

HAT-P-38b: A Saturn-Mass Planet Transiting a Late G Star

Bun'ei SATO¹ Joel D. HARTMAN^{2,3} Gáspár Á. BAKOS^{2,3} Bence BÉKY³ Guillermo TORRES³ David W. LATHAM³
Géza KOVÁCS⁴ Zoltán CSUBRY^{2,3} Kaloyan PENEV^{2,3} Robert W. NOYES³ Lars A. BUCHHAVE⁵ Samuel N. QUINN^{3,6}
Mark EVERETT³ Gilbert A. ESQUERDO³ Debra A. FISCHER⁷ Andrew W. HOWARD⁸ John A. JOHNSON⁹ Geoff W.
MARCY⁸ Dimitar D. SASSELOV³ Tamás SZKLENÁR³ József LÁZÁR¹⁰ István PAPP¹⁰ Pál SÁRI¹⁰

¹*Department of Earth and Planetary Sciences, Tokyo Institute of Technology, Tokyo, Japan*
satobn@geo.titech.ac.jp

²*Department of Astrophysical Sciences, Princeton University, Princeton, NJ, USA*

³*Harvard-Smithsonian Center for Astrophysics, Cambridge, MA, USA*

⁴*Konkoly Observatory, Budapest, Hungary*

⁵*Niels Bohr Institute, University of Copenhagen, DK-2100, Denmark, and Centre for Star and Planet Formation, Natural History Museum of Denmark, DK-1350 Copenhagen*

⁶*Department of Physics and Astronomy, Georgia State University, Atlanta, GA, USA*

⁷*Astronomy Department, Yale University, New Haven, CT*

⁸*Department of Astronomy, University of California, Berkeley, CA*

⁹*California Institute of Technology, Department of Astrophysics, MC 249-17, Pasadena, CA*

¹⁰*Hungarian Astronomical Association*

(Received ; accepted)

Abstract

We report the discovery of HAT-P-38b, a Saturn-mass exoplanet transiting the V=12.56 dwarf star GSC 2314-00559 on a $P = 4.6404$ d circular orbit. The host star is a $0.89 M_{\odot}$ late G-dwarf, with solar metallicity, and a radius of $0.92 R_{\odot}$. The planetary companion has a mass of $0.27 M_J$, and radius of $0.82 R_J$. HAT-P-38b is one of the closest planets in mass and radius to Saturn ever discovered.

Key words: planetary systems — stars: individual (HAT-P-38, GSC 2314-00559) — techniques: spectroscopic, photometric

1. Introduction

Transiting extrasolar planets (TEPs) provide unique opportunities to study the bulk physical properties (mass, radius, mean density) of planetary mass objects. These data can be compared with theoretical predictions based on planet interior models to give us insight into the formation and evolution of planets (e.g. Baraffe et al. 2008; Fortney et al. 2007; Burrows et al. 2007; Seager et al. 2007). To date, more than 150 TEPs identified by dedicated photometric surveys have been confirmed by dynamical mass determinations¹, and the planets have been found to show great diversity in their properties. For example, at the high-mass end Jupiter-mass and super-Jupiter-mass planets ($M \gtrsim 0.4 M_J$), which are most likely H/He-dominated gas giants, exhibit a wide range of radii and inferred core masses (e.g. Cabrera et al. 2010; Anderson et al. 2011). At the low-mass end ($M \lesssim 0.1 M_J$), super-Earths and Neptunes may have diversity in their bulk compositions (e.g. Valencia et al. 2010; Charbonneau et al. 2009; Lissauer et al. 2011).

In between, the sample size of known Saturn-mass TEPs ($0.1 < M < 0.4 M_J$)² is still quite small probably because these planets are intrinsically rare at short orbital periods

(Hartman et al. 2009). However, the 11 previously known Saturn-mass TEPs also appear to show diverse properties, like the more massive planets, with a wide range of mean densities, from 0.3 to 2.3 times that of Saturn ($\rho_p = 0.19 \text{ g cm}^{-3}$ for WASP-39b and $\rho_p = 1.6 \text{ g cm}^{-3}$ for CoRoT-8b, respectively; Faedi et al. 2011; Borde et al. 2010). A correlation between metallicity and inferred core mass (e.g. Hartman et al. 2009; Miller & Fortney 2011), and also between metallicity, irradiation (planetary equilibrium temperature), and planet radii has been suggested for the Saturn-mass TEPs (e.g. Enoch et al. 2011; Béky et al. 2011), but it should be confirmed by collecting a larger number of samples.

The Hungarian-made Automated Telescope Network (HATNet; Bakos et al. 2004) survey for transiting exoplanets (TEPs) around bright stars ($9 \lesssim r \lesssim 14.5$) operates six wide-field instruments: four at the Fred Lawrence Whipple Observatory (FLWO) in Arizona, and two on the roof of the hangar servicing the Smithsonian Astrophysical Observatory's Submillimeter Array, in Hawaii. Since 2006, HATNet has announced and published 37 TEPs (e.g. Hartman et al. 2011b). In this work we report our thirty-eighth discovery, around the relatively bright star GSC 2314-00559. HAT-P-38b is one of the closest planets in mass and radius to Saturn ever discovered.

In Section 2 we summarize the detection of the pho-

¹ e.g. <http://exoplanets.org>

² There is no strict definition of Saturn-mass planets. The mass range is somewhat arbitrarily set limit for these lighter TEPs.

ometric transit signal and the subsequent spectroscopic and photometric observations of HAT-P-38 to confirm the planet. In Section 3 we analyze the data to rule out false positive scenarios, and to determine the stellar and planetary parameters. Our findings are discussed in Section 4.

2. Observations

The observational procedure employed by HATNet to discover TEPs has been described in detail in several previous discovery papers (e.g. Bakos et al. 2010, Latham et al. 2009). In the following subsections we highlight specific details that are pertinent to the discovery of HAT-P-38b.

2.1. Photometric detection

The transits of HAT-P-38b were detected with the HAT-5 telescope in Arizona and the HAT-8 telescope in Hawaii. A total of 2381 exposures of 5 minutes and 6126 exposures of 3 minutes were obtained in Sloan r band for a $\sim 10^\circ \times 10^\circ$ field containing GSC 2314-00559 between August and November 2010. We reduced these observations to light curves for the 36,000 stars in the field with $r \lesssim 14.5$ whose positions were derived from the Two Micron All Sky Survey catalog (2MASS; Skrutskie et al. 2006) using a custom image subtraction (Alard 2000) based procedure with discrete kernels (Bramich 2008), as described in Pál (2009). After decorrelating against external parameters and detrending with the Trend Filtering Algorithm (TFA; Kovács et al. 2005), we achieved a per-image photometric precision of 3.5 mmag for the brightest stars in the field.

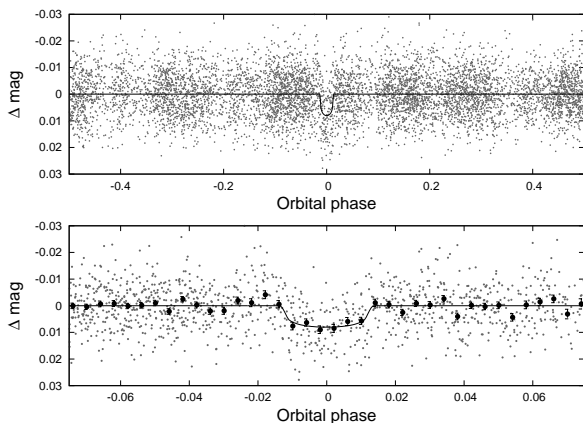


Fig. 1. Unbinned light curve of HAT-P-38 including all ~ 8500 instrumental r band measurements obtained with the HAT-5 and HAT-8 telescopes of HATNet (see the text for details), and folded with the period $P = 4.640382$ days resulting from the global fit described in Section 3. The solid line shows a simplified transit model fit to the light curve (Section 3.2). The bottom panel shows a zoomed-in view of the transit, the filled circles show the light curve binned in phase with a bin-size of 0.004.

The light curves were searched for transits using the Box Least-Squares (BLS; Kovács et al. 2002) method. We detected a significant signal in the light curve of GSC 2314-

00559 (also known as 2MASS 02213197+3214461; $\alpha = 02^{\text{h}}21^{\text{m}}31.97\text{s}$, $\delta = +32^\circ 14' 46.1''$; J2000; $V = 12.557 \pm 0.094$ Droege et al. 2006), with a period of $P = 4.6404$ days (see Figure 1).

2.2. Reconnaissance Spectroscopy

High-resolution, low-S/N reconnaissance spectra were obtained for HAT-P-38 using the Tillinghast Reflector Echelle Spectrograph (TRES; Fűrész 2008) on the 1.5 m Tillinghast Reflector at FLWO. Three TRES spectra of HAT-P-38 were obtained, reduced and analyzed to measure the stellar effective temperature, surface gravity, projected rotation velocity, and radial velocity (RV) via cross-correlation against a library of synthetic template spectra. For details see Quinn et al. (2012) and Buchhave et al. (2010). The resulting measurements are given in Table 1.

These observations revealed no detectable RV variation at the $\sim 0.1 \text{ km s}^{-1}$ precision of the observations. Additionally the spectra are consistent with a single, slowly-rotating, dwarf star.

2.3. High resolution, high S/N spectroscopy

We proceeded with the follow-up of this candidate by obtaining high-resolution, high-S/N spectra to detect and characterize RV variations induced by the putative planet. For this we used the High-Dispersion Spectrograph (HDS; Noguchi et al. 2002) with the I_2 absorption cell (Kambe et al. 2002) on the Subaru telescope. We obtained a total of 16 spectra, including two I_2 -free observations which we used to construct a template for the RV measurements. The observations were made on four nights between 2011 August 05 and 2011 August 08 using the KV370 filter, a $0''.6 \times 2''.0$ slit, giving a wavelength resolution ($\lambda/\Delta\lambda$) of 60000, and the StdI2b setup, covering a wavelength region of 3500–6200 Å. We used exposure times of 10 to 20 minutes, yielding a S/N per resolution element of 45 to 80 at 5500 Å, depending on seeing. The spectra were extracted and reduced to relative RVs in the solar system barycentric frame following the procedure of Sato et al. (2002) and Sato et al. (2005), which is based on the method by Butler et al. (1996). In this technique a star+ I_2 spectrum is modeled as a product of a high resolution I_2 and a stellar template spectrum convolved with a modeled instrumental profile (IP) of the spectrograph. To obtain the stellar template, Sato et al. (2002) extracted a high resolution stellar spectrum from several star+ I_2 spectra. However, we have since found that when applying this technique for obtaining a template for the HDS spectra systematic errors sometimes appear in the resulting RVs. These errors disappear when we use a stellar template obtained by deconvolving a pure stellar spectrum with the spectrograph IP estimated from a B-star+ I_2 spectrum. We applied this latter technique to generate the template for our HDS observations of HAT-P-38. The resulting RV measurements and their uncertainties are listed in Table 2. The period-folded data, along with our best fit described below in Section 3, are displayed in Figure 2.

In addition to the HDS/Subaru observations, we also obtained a single high-resolution, high-S/N spectrum us-

Table 1. Reconnaissance Spectroscopy of HAT-P-38 with TRES.

HJD (2,455,000+)	T_{eff} (K)	$\log g$ (cgs)	$v \sin i$ (kms^{-1})	RV (kms^{-1})
546.66915	5510	4.57	2.4	-19.60
576.59133	5460	4.49	2.5	-19.83
578.64318	5420	4.39	2.4	-19.72

Uncertainties on T_{eff} , $\log g$, $v \sin i$, and the RV are ~ 100 K, 0.1 dex, 0.5 kms^{-1} , and $\sim 0.1 \text{ kms}^{-1}$, respectively. The stellar parameters were derived with the assumption of $[\text{Fe}/\text{H}] = 0.0$.

ing the HIRES instrument (Vogt et al. 1994) on the Keck I telescope. This observation was made without the I_2 absorption cell on the night of 2011 February 19, and was used to determine the stellar parameters as described in Section 3.1.

A bisector analysis based on the HDS spectra was done following a procedure similar to that described in Section 5 of Bakos et al. (2007b). The resulting bisector spans, plotted in Figure 2, show no significant variation, and are not correlated with the RVs. The combination of no detectable bisector span variations, RV variations consistent with a Keplerian orbit in phase with the photometric ephemeris, and short ingress and egress durations relative to the full transit duration (Section 2.4), is strong evidence that HAT-P-38 is not a blend, but rather a real TEP system.

In the same figure we also show the relative S index (Vaughan, Preston & Wilson 1978), which is a measure of the chromospheric activity of the star derived from the flux in the cores of the CaII H and K lines. Note that our relative S index has not been calibrated to the scale of Vaughan, Preston & Wilson (1978). Following Isaacson & Fischer (2010), we measured $S_{\text{HK}} = 0.144$ on the calibrated scale using the Keck/HIRES iodine-free observation. This corresponds to a bolometric flux-corrected activity measure of $\log R'_{\text{HK}} = -5.124$ using the definition of Noyes et al. (1984). The star is inactive, consistent with its slow projected rotation velocity.

2.4. Photometric follow-up observations

In order to accurately characterize the system, we conducted additional photometric observations with the KeplerCam CCD camera on the FLWO 1.2m telescope. Observations were performed on the nights of 2011 September 25, and 2011 November 1, in both cases using a Sloan i filter. On the first night we used an exposure time of 100 s, on the second night we used an exposure time of 90 s. Due to the limited accuracy of the ephemeris calculated from the HATNet data the transit occurred earlier than expected on 2011 September 25, so that only the end of egress was observed. We used this data to revise the ephemeris so that a full transit was observed on the night of 2011 November 01.

The reduction of these images, including basic calibration, astrometry, and aperture photometry, was performed in a similar fashion to previous HATNet discov-

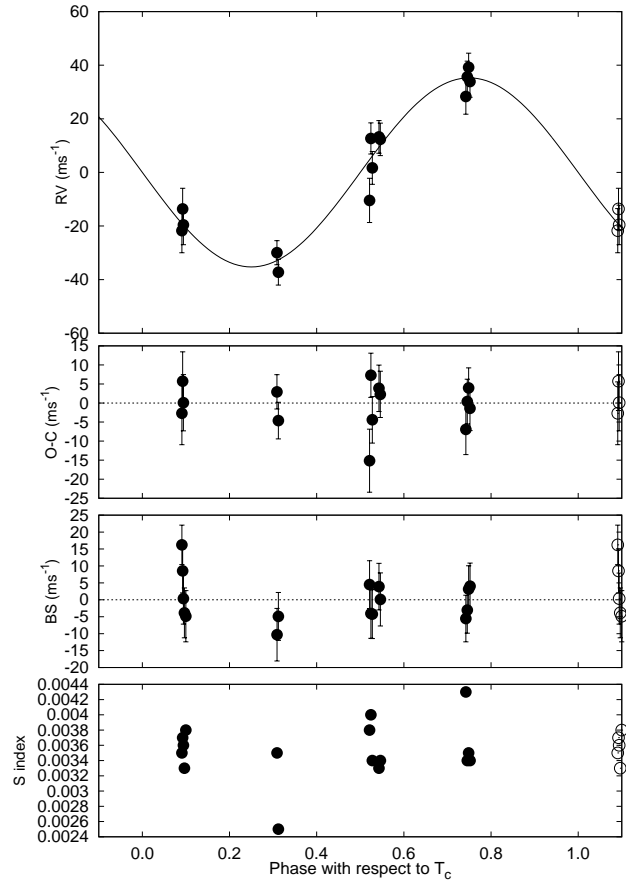


Fig. 2. *Top panel:* Subaru/HDS RV measurements for HAT-P-38 shown as a function of orbital phase, along with our best-fit model (see Table 5). Zero phase corresponds to the time of mid-transit. The center-of-mass velocity has been subtracted. *Second panel:* Velocity $O-C$ residuals from the best fit. *Third panel:* Bisector spans (BS) for the HDS spectra, with the mean value subtracted. The measurement from the template spectrum is included (see Section 2.3). *Bottom panel:* Relative chromospheric activity index S measured from the HDS spectra. Note the different vertical scales of the panels. Observations shown twice are represented with open circles.

eries (Bakos et al. 2010). We used the “ELTG” model described in Bakos et al. (2010) to remove trends simultaneously with the light curve modeling. The final time series are shown in the top portion of Figure 3, along with

Table 2. Relative radial velocities, bisector spans, and activity index measurements of HAT-P-38 from HDS/Subaru.

BJD ^a (2,454,000+)	RV ^b (ms ⁻¹)	σ_{RV} (ms ⁻¹)	BS (ms ⁻¹)	σ_{BS} (ms ⁻¹)	S ^c	Phase
1780.01380	-21.74	8.25	16.23	5.83	0.0035	0.091
1780.02157	-13.63	7.70	8.53	6.48	0.0037	0.092
1780.02933	-19.59	7.38	0.36	7.53	0.0036	0.094
1780.04091	-3.86	7.37	0.0033	0.097
1780.05562	-4.85	7.56	0.0038	0.100
1781.02601	-29.96	4.50	-10.30	7.76	0.0035	0.309
1781.04075	-37.24	4.80	-4.91	7.07	0.0025	0.312
1782.01133	-10.45	8.27	4.49	7.05	0.0038	0.521
1782.02606	12.66	5.81	-4.07	7.29	0.0040	0.524
1782.04078	1.68	6.12	-4.23	7.21	0.0034	0.528
1782.11167	13.24	6.10	3.90	6.88	0.0033	0.543
1782.12638	12.33	6.07	0.10	7.83	0.0034	0.546
1783.03706	28.32	6.61	-5.54	6.88	0.0043	0.742
1783.05178	35.64	5.88	-3.03	6.83	0.0034	0.745
1783.06650	39.23	5.27	3.16	6.89	0.0035	0.749
1783.08123	33.89	5.84	4.03	6.82	0.0034	0.752

^aBarycentric Julian dates throughout the paper are calculated from Coordinated Universal Time (UTC).

^bThe zero-point of these velocities is arbitrary. An overall offset γ_{rel} fitted to these velocities in Section 3.2 has *not* been subtracted.

^cRelative chromospheric activity index, not calibrated to the scale of Vaughan, Preston & Wilson (1978).

For the iodine-free template exposures there is no RV measurement, but the BS and S index can still be determined.

our best-fit transit light curve model described below; the individual measurements are reported in Table 3.

3. Analysis

The analysis of the HAT-P-38 system, including determinations of the properties of the host star and planet, was carried out in a similar fashion to previous HATNet discoveries. Below we briefly summarize the procedure and the results for HAT-P-38.

3.1. Properties of the parent star

Stellar atmospheric parameters were measured using our template spectrum obtained with the Keck/HIRES instrument, and the analysis package known as Spectroscopy Made Easy (SME; Valenti & Piskunov 1996), along with the atomic line database of Valenti & Fischer (2005). SME yielded the following values and uncertainties: effective temperature $T_{eff\star} = 5330 \pm 100$ K, metallicity $[Fe/H] = +0.06 \pm 0.1$ dex, stellar surface gravity $\log g_{\star} = 4.42 \pm 0.1$ (cgs), and projected rotation velocity $v \sin i = 0.4 \pm 0.5$ km s⁻¹.

The values of $T_{eff\star}$, $\log g_{\star}$, and $[Fe/H]$ were used to determine the limb-darkening coefficients needed in the global modeling of the follow-up photometry. Following Sozzetti et al. (2007) we used a/R_{\star} , the normalized semi-major axis, rather than the surface gravity estimated from the spectrum, in determining the physical stellar parameters. We combined a/R_{\star} , $T_{eff\star}$, and $[Fe/H]$ with stellar evolution models from the Yonsei-Yale (YY) series by

Yi et al. (2001) to determine probability distributions of other stellar properties, including $\log g_{\star}$. The result for the surface gravity, $\log g_{\star} = 4.45 \pm 0.08$, is consistent with the value from our SME analysis, so we did not perform an additional iteration of SME with a fixed surface gravity.

We find that HAT-P-38 has a stellar mass and radius of $M_{\star} = 0.886 \pm 0.044 M_{\odot}$ and $R_{\star} = 0.923_{-0.067}^{+0.096} R_{\odot}$, respectively. These, along with other properties, are listed in Table 4. We find that the system has an age greater than 1.7 Gyr with 95% confidence. We show the inferred location of the star in a diagram of a/R_{\star} versus $T_{eff\star}$, analogous to the classical H-R diagram, in Figure 4.

3.2. Global modeling of the data

We modeled the HATNet photometry, the follow-up photometry, and the high-precision RV measurements using the procedure described in detail by Bakos et al. (2010).

The resulting parameters pertaining to the light curves and RV curves, together with derived physical parameters of the planet, are listed in Table 5.

We find a mass for the planet of $M_p = 0.267 \pm 0.020 M_J$ and a radius of $R_p = 0.825_{-0.063}^{+0.092} R_J$, leading to a mean density $\rho_p = 0.59 \pm 0.16$ g cm⁻³. These and other planetary parameters are listed at the bottom of Table 5. We note that the eccentricity of the orbit is consistent with zero: $k \equiv e \cos(\omega) = 0.003 \pm 0.028$ and $h \equiv e \sin(\omega) = -0.018 \pm 0.083$ ($e = 0.067 \pm 0.047$, $\omega = 240 \pm 104^\circ$). We find $e < 0.165$ with 95% confidence.

Table 3. Differential photometry of HAT-P-38

BJD (2,400,000+)	Mag ^a	σ_{Mag}	Mag(orig) ^b	Filter
55830.68887	0.00786	0.00085	11.10930	<i>i</i>
55830.69021	0.00339	0.00084	11.10510	<i>i</i>
55830.69152	0.00650	0.00084	11.10810	<i>i</i>
55830.69282	0.00256	0.00084	11.10410	<i>i</i>
55830.69414	0.00271	0.00084	11.10430	<i>i</i>
55830.69546	0.00338	0.00084	11.10500	<i>i</i>
55830.69678	0.00228	0.00084	11.10360	<i>i</i>
55830.69808	0.00251	0.00084	11.10380	<i>i</i>
55830.69939	-0.00047	0.00083	11.10140	<i>i</i>
55830.70071	0.00058	0.00083	11.10240	<i>i</i>

^aThe out-of-transit level has been subtracted. These magnitudes have been processed with the EPD and TFA procedures.

^bRaw magnitude values without application of the EPD and TFA procedures.

This table is available in a machine-readable form in the online journal. A portion is shown here for guidance regarding its form and content.

4. Discussion

HAT-P-38b belongs to the small, but increasing group of Saturn-mass planets ($0.1 < M < 0.4M_J$; Figure 5; Table 6). Of the 12 known Saturn-mass TEPs, HAT-P-38b is the planet closest in mass and radius to Saturn, along with WASP-29b ($M_p = 0.244 \pm 0.020 M_J$, $R_p = 0.792^{+0.056}_{-0.035} R_J$, $\rho_p = 0.65 \pm 0.10 \text{ g cm}^{-3}$; Hellier et al. 2010) and the somewhat lower density planets Kepler-9b and Kepler-9c ($\rho_p \sim 0.4\text{--}0.5 \text{ g cm}^{-3}$; Holman et al. 2010). Other Saturn-mass TEPs include the inflated, low-density ($\rho_p \sim 0.3 \text{ g cm}^{-3}$) planets HAT-P-12b (Hartman et al. 2009), HAT-P-18b, HAT-P-19b (Hartman et al. 2011a), WASP-21b (Bouchy et al. 2010), and WASP-39b (Faedi et al. 2011), and the dense planets CoRoT-8b (Borde et al. 2010), Kepler-16ABb (Doyle et al. 2011), and HD 149026b (Sato et al. 2005) with $\rho_p \gtrsim 0.9 \text{ g cm}^{-3}$.

For $0.1\text{--}0.6 M_J$ planets, Enoch et al. (2011) find that planetary radius is proportional to planetary equilibrium temperature and inversely proportional to host star metallicity, with hotter planets having more inflated radii and planets orbiting lower metallicity stars have larger radii (perhaps because they have smaller metal-rich cores). The observed radius for HAT-P-38b is slightly smaller than that expected from the relationship ($0.83 R_J$ compared to the expected value of $0.97 R_J$ based on the equation (3) in Enoch et al. 2011), but is still consistent with the general trend.

HAT-P-38b provides a clear example that irradiation is not the sole factor affecting the radii of Saturn-mass planets as it has a higher planetary equilibrium temperature ($T_{\text{eq}} = 1082 \text{ K}$) than that of inflated planets such as HAT-P-12b ($R_p = 0.959 R_J$, $T_{\text{eq}} = 963 \text{ K}$) and HAT-P-18b ($R_p = 0.995 R_J$, $T_{\text{eq}} = 852 \text{ K}$). Metallicity is clearly another important factor in setting the radii of planets in this mass range. From the theoretical models of Fortney et

al. (2007), HAT-P-38b could have a heavy-element core of $\sim 25 M_{\oplus}$, fitting the general trend that higher-metallicity systems have larger inferred cores and thus smaller planetary radii. However, the recently discovered planets violate this pattern; HAT-P-18b and HAT-P-19b have low densities even with high metallicity ($[\text{Fe}/\text{H}] = +0.10$ and $+0.23$, respectively), while the circumbinary planet Kepler-16ABb has a high density even with low metallicity ($[\text{m}/\text{H}] = -0.3$), suggesting that the relationship is not so simple. Continued discoveries over a wide range of planetary and stellar parameters will allow us to further investigate the nature of these Saturn-mass planets.

HATNet operations have been funded by NASA grants NNG04GN74G, NNX08AF23G, NNX09AB29G and SAO IR&D grants. GT acknowledges partial support from NASA grant NNX09AF59G. We acknowledge partial support also from the Kepler Mission under NASA Cooperative Agreement NCC2-1390 (D.W.L., PI). G.K. thanks the Hungarian Scientific Research Foundation (OTKA) for support through grant K-81373. This research has made use of Keck telescope time granted through NASA (N108Hr). Based in part on data collected at Subaru Telescope, which is operated by the National Astronomical Observatory of Japan.

References

- Alard, C. 2000, A&AS, 144, 363
Anderson, D. R., Simth, A. M. S., Lanotte, A. A., et al. 2011, MNRAS, 416, 2108
Bramich, D. M. 2008, MNRAS, 386, L77
Bakos, G. Á., Noyes, R. W., Kovács, G., Stanek, K. Z., Sasselov, D. D., & Domsa, I. 2004, PASP, 116, 266
Bakos, G. Á., et al. 2007a, ApJ, 656, 552
Bakos, G. Á., et al. 2007b, ApJ, 670, 826
Bakos, G. Á., et al. 2010, ApJ, 710, 1724

Table 4. Stellar parameters for HAT-P-38

Parameter	Value	Source
Spectroscopic properties		
$T_{\text{eff}\star}$ (K).....	5330 ± 100	SME ^a
[Fe/H].....	$+0.06 \pm 0.1$	SME
$v \sin i$ (kms ⁻¹)..	0.4 ± 0.5	SME
v_{mac} (kms ⁻¹)..	3.33	SME
v_{mic} (kms ⁻¹)..	0.85	SME
γ_{RV} (kms ⁻¹)..	-19.7 ± 0.1	TRES
$\log R'_{\text{HK}}$	-5.124	HIRES
Photometric properties		
V (mag).....	12.557 ± 0.094	TASS
$V - I_C$ (mag) ..	0.87 ± 0.13	TASS
J (mag).....	10.989 ± 0.022	2MASS
H (mag).....	10.593 ± 0.021	2MASS
K_s (mag).....	10.501 ± 0.017	2MASS
Derived properties		
M_{\star} (M_{\odot}).....	0.886 ± 0.044	YY+a/ R_{\star} +SME ^b
R_{\star} (R_{\odot}).....	$0.923^{+0.096}_{-0.067}$	YY+a/ R_{\star} +SME
$\log g_{\star}$ (cgs)....	4.45 ± 0.08	YY+a/ R_{\star} +SME
L_{\star} (L_{\odot}).....	$0.62^{+0.16}_{-0.10}$	YY+a/ R_{\star} +SME
M_V (mag).....	5.44 ± 0.24	YY+a/ R_{\star} +SME
M_K (mag,ESO)	3.56 ± 0.20	YY+a/ R_{\star} +SME
Age (Gyr).....	10.1 ± 4.8	YY+a/ R_{\star} +SME
Distance (pc) ^c ..	249^{+26}_{-19}	YY+a/ R_{\star} +SME

^aSME = ‘‘Spectroscopy Made Easy’’ package for the analysis of high-resolution spectra (Valenti & Piskunov 1996).

^bYY+a/ R_{\star} +SME = Based on the YY isochrones (Yi et al. 2001), a/R_{\star} as a luminosity indicator, and the SME results.

^cDetermined by comparing the 2MASS K_s magnitude to the predicted absolute M_K magnitude.

- Baraffe, I., Chabrier, G., & Barman, T., 2008, A&A, 482, 315
- Béky, B., et al. 2011, ApJ, 734, 109
- Bord é, P., et al. 2010, A&A, 520, 66
- Bouchy, F., et al. 2010, A&A, 519, 98
- Buchhave, L. A., et al. 2010, ApJ, 720, 1118
- Burrows, A., Hubeny, I., Budaj, J., & Hubbard, W.B. 2007, ApJ, 661, 502
- Butler, R.P., Marcy, G.W., Williams, E., McCarthy, C., Dosanji, P., & Vogt, S.S. 1996, PASP, 108, 500
- Cabrera, J. et al., 2010, A&A, 522, 110
- Carter, J. A., Winn, J. N., Gilliland, R., & Holman, M. J. 2009, ApJ, 696, 241
- Charbonneau, D., et al. 2009, Nature, 462, 891
- Claret, A. 2004, A&A, 428, 1001
- Doyle, L. R. A. et al. 2011, Science, 333, 1602
- Droege, T. F., Richmond, M. W., & Sallman, M. 2006, PASP, 118, 1666
- Enoch, B., et al. 2011, MNRAS, 410, 1631
- Faedi, F., et al. 2011, A&A, 531, 40
- Fortney, J. J., Marley, M. S., & Barnes, J. W. 2007, ApJ, 659, 1661
- Fűrész, G. 2008, Ph.D. thesis, University of Szeged, Hungary
- Hansen, B. M. S., & Barman, T. 2007, ApJ, 671, 861
- Hartman, J. D., et al. 2009, ApJ, 706, 785
- Hartman, J. D., et al. 2011a, ApJ, 726, 52
- Hartman, J. D., et al. 2011b, ApJ, 742, 59
- Havel, M., Guillot, T., Valencia, D., & Crida, A. 2011, A&A, 531, 11
- Hellier, C., et al. 2010, ApJ, 723, 60
- Holman, M. J., et al. 2010, Science, 330, 51
- Isaacson, H., & Fischer, D. 2010, ApJ, 725, 875
- Kambe, E. et al. 2002, PASJ, 54, 865
- Kovács, G., Zucker, S., & Mazeh, T. 2002, A&A, 391, 369
- Kovács, G., Bakos, G. Á., & Noyes, R. W. 2005, MNRAS, 356, 557
- Latham, D. W., et al. 2009, ApJ, 704, 1107
- Lissauer, J. J., et al. 2011, Nature, 570, 53
- Miller, N. & Fortney, J. J. 2011, ApJ, 736, L29
- Noguchi, N., et al. 2002, PASJ, 54, 819
- Noyes, R. W., Hartmann, L. W., Baliunas, S. L., Duncan, D. K., & Vaughan, A. H. 1984, ApJ, 279, 763
- Pál, A. 2009, arXiv:0906.3486, PhD thesis
- Quinn, S., et al. 2012, ApJ, 745, 80
- Sato, B., Kambe, E., Takeda, T., Izumiura, H., & Ando, H. 2002, PASJ, 54, 873
- Sato, B., et al. 2005, ApJ, 633, 465
- Seager, S., Kuchner, M., Hier-Majumder, C. A., & Militzer, B. 2007, ApJ, 669, 1279
- Skrutskie, M. F., et al. 2006, AJ, 131, 1163
- Sozzetti, A. et al. 2007, ApJ, 664, 1190
- Valencia, D., et al. 2010, A&A, 516, 20
- Valenti, J. A., & Fischer, D. A. 2005, ApJS, 159, 141
- Valenti, J. A., & Piskunov, N. 1996, A&AS, 118, 595

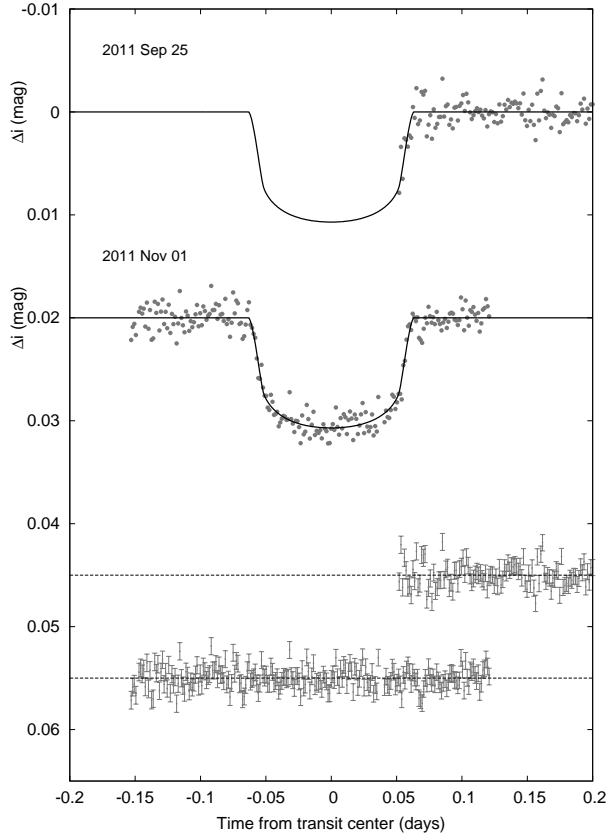


Fig. 3. Unbinned instrumental *i* band transit light curves, acquired with KeplerCam at the FLWO 1.2 m telescope. The light curves have been EPD- and TFA-processed, as described in § 3.2. The dates of the events are indicated. Curves after the first are displaced vertically for clarity. Our best fit from the global modeling described in Section 3.2 is shown by the solid lines. Residuals from the fits are displayed at the bottom, in the same order as the top curves. The error bars represent the photon and background shot noise, plus the readout noise.

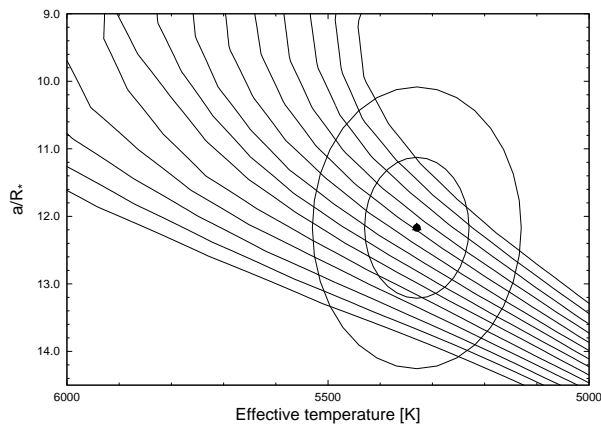


Fig. 4. Model isochrones from Yi et al. (2001) for the measured metallicity of HAT-P-38, $[\text{Fe}/\text{H}] = +0.06$, and ages of 1 to 14 Gyr in steps of 1 Gyr (left to right). The adopted values of $T_{\text{eff}\star}$ and a/R_{\star} are shown together with their 1- σ and 2- σ confidence ellipsoids.

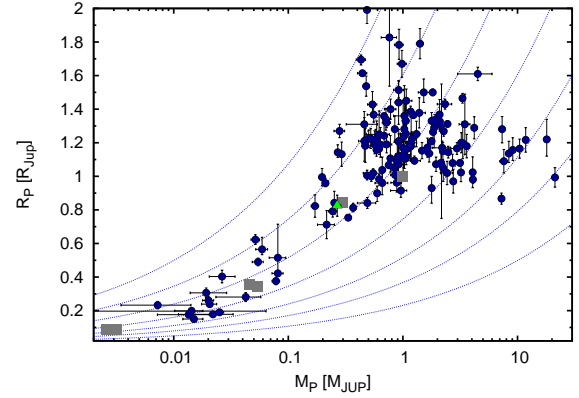


Fig. 5. Mass–radius diagram of known TEPs (blue circles). HAT-P-38b is shown as a green triangle. Overlaid are isodensity lines for 0.1, 0.3, 0.9, 3.0, 9.0, 25.0, and 100 g cm^{-3} (dotted lines). Solar system planets are shown with gray squares.

Vogt, S. S. et al. 1994, Proc. SPIE, 2198, 362

Yi, S. K. et al. 2001, ApJS, 136, 417

Vaughan, A. H., Preston, G. W., & Wilson, O. C. 1978, PASP, 90, 267

Table 5. Orbital and planetary parameters

Parameter	Value
Light curve parameters	
P (days)	4.640382 ± 0.000032
T_c (BJD) ^a	$2455863.11957 \pm 0.00035$
T_{14} (days) ^a	0.1267 ± 0.0015
$T_{12} = T_{34}$ (days) ^a	0.0122 ± 0.0013
a/R_*	12.17 ± 1.04
ζ/R_* ^b	17.46 ± 0.12
R_p/R_*	0.0918 ± 0.0016
b^2	$0.139^{+0.083}_{-0.072}$
$b \equiv a \cos i/R_*$	$0.372^{+0.094}_{-0.132}$
i (deg)	88.3 ± 0.7
Limb-darkening coefficients^c	
a_i (linear term, i filter)	0.3464
b_i (quadratic term)	0.2857
RV parameters	
K (ms^{-1})	35.4 ± 2.4
k_{RV} ^d	0.003 ± 0.028
h_{RV} ^d	-0.018 ± 0.083
e	0.067 ± 0.047
ω (deg)	240 ± 104
RV fit RMS (ms^{-1})	5.7
Secondary eclipse parameters	
T_s (BJD)	2455865.449 ± 0.083
$T_{s,14}$	0.1229 ± 0.0176
$T_{s,12}$	0.0117 ± 0.0029
Planetary parameters	
M_p (M_J)	0.267 ± 0.020
R_p (R_J)	$0.825^{+0.092}_{-0.063}$
$C(M_p, R_p)$ ^e	0.18
ρ_p (g cm^{-3})	0.59 ± 0.16
$\log g_p$ (cgs)	2.99 ± 0.08
a (AU)	0.0523 ± 0.0009
T_{eq} (K)	1082 ± 55
Θ ^f	0.038 ± 0.004
$\langle F \rangle$ ($10^8 \text{ergs}^{-1} \text{cm}^{-2}$) ^g	$3.09^{+0.80}_{-0.50}$

^a T_c : Reference epoch of mid transit that minimizes the correlation with the orbital period. BJD is calculated from UTC. T_{14} : total transit duration, time between first to last contact; $T_{12} = T_{34}$: ingress/egress time, time between first and second, or third and fourth contact.

^b The reciprocal of the half duration of the transit, related to a/R_* , is used as a jump parameter in the MCMC procedure.

^c Values for a quadratic law, adopted from the tabulations by Claret (2004) according to the spectroscopic (SME) parameters listed in Table 4.

^d $k_{\text{RV}} = e \cos \omega$ and $h_{\text{RV}} = e \sin \omega$. These are determined from the global modeling, and primarily constrained by the RV data.

^e Correlation coefficient between the planetary mass M_p and radius R_p .

^f The Safronov number is given by $\Theta = \frac{1}{2}(V_{\text{esc}}/V_{\text{orb}})^2 = (a/R_p)(M_p/M_*)$ (see Hansen & Barman 2007).

^g Incoming flux per unit surface area, averaged over the orbit.

Table 6. Saturn-mass TEPs ($0.1 < M < 0.4M_J$)

Planet Name	Mass (M_J)	Radius (R_J)	Mean Density (g cm^{-3})	T_{eq}^{a} (K)	[Fe/H]	Reference
Kepler-9c	0.171±0.013	0.823±0.067	0.383±0.098	620±30	–	Holman et al. (2010) Havel et al. (2011)
HAT-P-18b	0.197±0.013	0.995±0.052	0.25±0.04	852±28	+0.10±0.08	Hartman et al. (2011a)
HAT-P-12b	0.211±0.012	0.959 ^{+0.029} _{-0.021}	0.295±0.025	963±16	–0.29±0.05	Hartman et al. (2009)
CoRoT-8b	0.22±0.03	0.57±0.02	1.6±0.1	860±20	+0.3±0.1 ^b	Borde et al. (2010)
WASP-29b	0.244±0.020	0.792 ^{+0.056} _{-0.035}	0.65±0.10	980±40	+0.11±0.14	Hellier et al. (2010)
Kepler-9b	0.252±0.013	0.842±0.069	0.524±0.132	780±30	–	Holman et al. (2010) Havel et al. (2011)
HAT-P-38b	0.267±0.020	0.825 ^{+0.092} _{-0.063}	0.59±0.16	1082±55	+0.06±0.1	This work
WASP-39b	0.28±0.03	1.27±0.04	0.19±0.03	1116 ⁺³³ ₋₃₂	–0.12±0.10	Faedi et al. (2011)
HAT-P-19b	0.292±0.018	1.132±0.072	0.25±0.04	1010±42	+0.23±0.08	Hartman et al. (2011a)
WASP-21b	0.300±0.011	1.07±0.06	0.32±0.07	1260±30	–0.46±0.11	Bouchy et al. (2010)
Kepler-16ABb	0.333±0.016	0.7538 ^{+0.0026} _{-0.0023}	0.964 ^{+0.047} _{-0.046}	206±7	–0.3±0.2 ^b	Doyle et al. (2011)
HD149026b	0.368 ^{+0.013} _{-0.014}	0.813 ^{+0.027} _{-0.025}	0.85 ^{+0.10} _{-0.09}	1740±60	+0.36±0.05	Sato et al. (2005) Carter et al. (2009)

^aPlanetary Bond albedo $A = 0$ is assumed.^bThe value is not [Fe/H] but [m/H].